

**Ubiquitous Spin-Orbit Coupling in a Screw Dislocation with High Spin Coherency**Lin Hu,<sup>1</sup> Huaqing Huang,<sup>2</sup> Zhengfei Wang,<sup>3</sup> W. Jiang,<sup>2</sup> Xiaojuan Ni,<sup>2</sup> Yinong Zhou,<sup>2</sup>  
V. Zielasek,<sup>4,‡</sup> M. G. Lagally,<sup>4</sup> Bing Huang,<sup>1,\*</sup> and Feng Liu<sup>2,5,†</sup><sup>1</sup>*Beijing Computational Science Research Center, Beijing 100193, China*<sup>2</sup>*Department of Materials Science and Engineering, University of Utah, Salt Lake City, Utah 84112, USA*<sup>3</sup>*Hefei National Laboratory for Physical Sciences at the Microscale, University of Science and Technology of China, Hefei, Anhui 230026, China*<sup>4</sup>*Department of Materials Science and Engineering, University of Wisconsin, Madison, Wisconsin 53706, USA*<sup>5</sup>*Collaborative Innovation Center of Quantum Matter, Beijing 100084, China*

(Received 26 January 2018; revised manuscript received 12 June 2018; published 6 August 2018)

We theoretically demonstrate that screw dislocation (SD), a 1D topological defect widely present in semiconductors, exhibits ubiquitously a new form of spin-orbit coupling (SOC) effect. Differing from the widely known conventional 2D Rashba-Dresselhaus (RD) SOC effect that typically exists at surfaces or interfaces, the deep-level nature of SD-SOC states in semiconductors readily makes it an ideal SOC. Remarkably, the spin texture of 1D SD-SOC, pertaining to the inherent symmetry of SD, exhibits a significantly higher degree of spin coherency than the 2D RD-SOC. Moreover, the 1D SD-SOC can be tuned by ionicity in compound semiconductors to ideally suppress spin relaxation, as demonstrated by comparative first-principles calculations of SDs in Si/Ge, GaAs, and SiC. Our findings therefore open a new door to manipulating spin transport in semiconductors by taking advantage of an otherwise detrimental topological defect.

DOI: [10.1103/PhysRevLett.121.066401](https://doi.org/10.1103/PhysRevLett.121.066401)

Spintronics offers a promising paradigm shift for future information and energy technologies by processing the electron spin instead of charge degree of freedom, thereby essentially avoiding heat dissipation. In a crystalline solid, the motion of an electron is inevitably coupled with its spin orientation through the spin-orbit coupling (SOC) effect. Therefore, discovering new forms of the SOC effect that provide more effective means to manipulate spin transport properties is not only of fundamental interest but also critical to the development of spintronics devices. In this Letter, we demonstrate a surprising form of SOC that exists ubiquitously in a screw dislocation (SD) in semiconductors.

The structural, mechanical, and electronic properties of dislocations have been intensively studied for decades [1–7]. They fall into three categories, i.e., edge, mixed, and screw type [1,2]. Recently, in a topological insulator, a dislocation has been shown to conduct topological edge states [8]. Also, the concept of quantum dislocation [6,7] has been introduced to account for their effect on superconducting transition temperature. In general, however, dislocations are considered to have a negative impact on materials properties and functionalities. For example, formation of dislocation is the leading mechanism for growth instability of coherent thin films [9]. Dislocations may create scattering centers [3–5] to lower carrier mobility, cause current leakage and act as in-gap deep-level carrier recombination centers [10–12]. Therefore, much research effort in the past has been devoted to alleviating dislocations in semiconductors.

Defying the conventional wisdom, here we turn the ordinarily harmful dislocations into something useful through a previously unknown SOC effect.

The extrinsic SOC effect (in contrast to the atomic SOC effect) in a crystal requires breaking of inversion symmetry, which commonly occurs on surfaces or interfaces as manifested by the 2D Rashba and Dresselhaus SOC (RD-SOC) effects [13,14]. Bulk RD-SOC was only found in polar materials, such as BiTeI [15] and ferroelectric semiconductors [16–17], which intrinsically lack inversion symmetry. The SOC we found in a SD is 1D in nature and exists in bulk materials, so it goes much beyond the conventional 2D RD-SOC effect. The RD-SOC effect has been widely exploited in spintronics devices, but met two main challenges. First, the spin-polarized SOC states are often not ideal, because they overlap with other spin-unpolarized bulk states around the Fermi energy [18–23]. Second, the spin texture is diverse, suffering from spin randomization (relaxation) due to momentum-changing electron scattering, and special combination of the RD-SOC effects is needed to produce an ideal spin texture to suppress spin relaxation [24]. Thus, an ideal SOC effect would transport the spin current with a fixed spin orientation (high spin coherency), without interference from other spin-unpolarized electrons and immune to changing electron momentum (direction).

The 1D SOC in a SD is inherently induced by breaking of local inversion symmetry along the dislocations core,

because the SD assumes always a rotational plus a fractional translational symmetry and generates a 1D spiral-type effective electrical field. Most importantly, the 1D SD-SOC resides deep in the band gap of semiconductors, completely isolated from the bulk bands. It has also an spin texture with a much higher degree of spin coherency than the 2D RD-SOC, which is tunable by the ionicity of a compound semiconductor, as demonstrated by first-principles calculations of several representative semiconductors (Si/Ge, GaAs, and SiC). Therefore, the 1D SD-SOC exhibits two *ideal* features that are not only fundamentally interesting but also highly desirable for spintronics device applications.

We first introduce the key features of the coherent 1D SD-SOC effect and highlight its main difference from a conventional 2D RD-SOC effect, as illustrated in Fig. 1. In general, the SOC in a crystal can be described by a Hamiltonian  $H_{\text{SOC}} = (\alpha/\hbar)(\mathbf{E} \times \mathbf{p}) \cdot \boldsymbol{\sigma}$  and  $\mathbf{E} = \nabla V$ , where  $\alpha$  is the material-dependent SOC constant,  $\hbar$  is the Plank constant,  $\mathbf{E}$  is the effective field induced by gradient of potential ( $V$ ),  $\mathbf{p}$  is the momentum, and  $\boldsymbol{\sigma} = (\sigma_x, \sigma_y, \sigma_z)$  are the Pauli matrices. For a system with  $C_{2v}$  rotational symmetry, a 2D RD-SOC Hamiltonian is derived as [25]

$$H_{\text{RD}}^{\text{2D}} = \lambda_R(k_y\sigma_x - k_x\sigma_y) + \lambda_D(k_x\sigma_x - k_y\sigma_y), \quad (1)$$

where  $k_x$  and  $k_y$  are the reciprocal-space wave vectors, and  $\lambda_R$  ( $\lambda_D$ ) are the Rashba (Dresselhaus) SOC strength. The first Rashba term usually arises at a surface or interface [26,27], where there exists a  $k$ -independent effective electric field in the direction perpendicular to the surface or interface, i.e.,  $\mathbf{E} = e\hat{z}$ . Then the spin-polarized bands adopt a 2D spin texture in the  $(k_x, k_y)$  plane as shown in Fig. 1(a). The second linear Dresselhaus term arises in an asymmetric quantum well or a strained zinc-blende film [28], where there is no macroscopic “net” field but effective  $k$ -dependent local fields,  $\mathbf{E}(-k_x, k_y) = \mathbf{E}(k_x, -k_y) = e\hat{z}$  and  $\mathbf{E}(k_x, k_y) = \mathbf{E}(-k_x, -k_y) = -e\hat{z}$ , and a 2D spin texture in the  $(k_x, k_y)$  plane as shown in Fig. 1(b). In a system with both terms of equal strength, the spin texture has a  $k$ -independent spin orientation as shown in Fig. 1(c).

In a SD, the potential  $V$  and hence the effective field  $\mathbf{E}$  must follow the structural symmetry of the SD. Taking the general twofold screw rotation symmetry along the  $c$  axis  $\hat{S} = \{C_2|(c/2)\}$ , the potential becomes  $V = V(\cos \vartheta, \sin \vartheta)$ , where  $\vartheta = [2\pi/(c/2)]z = 2G_z z$ . After some algebra (see Supplemental Material [29]), a general 1D SD-SOC Hamiltonian can be expressed as

$$H_{\text{SD}}^{\text{1D}} = \lambda_e k_z \left( \cos \frac{k_z}{2} \sigma_y - \sin \frac{k_z}{2} \sigma_x \right) + \lambda_c k_z \left( \cos \frac{k_z}{2} \sigma_x - \sin \frac{k_z}{2} \sigma_y \right), \quad (2)$$

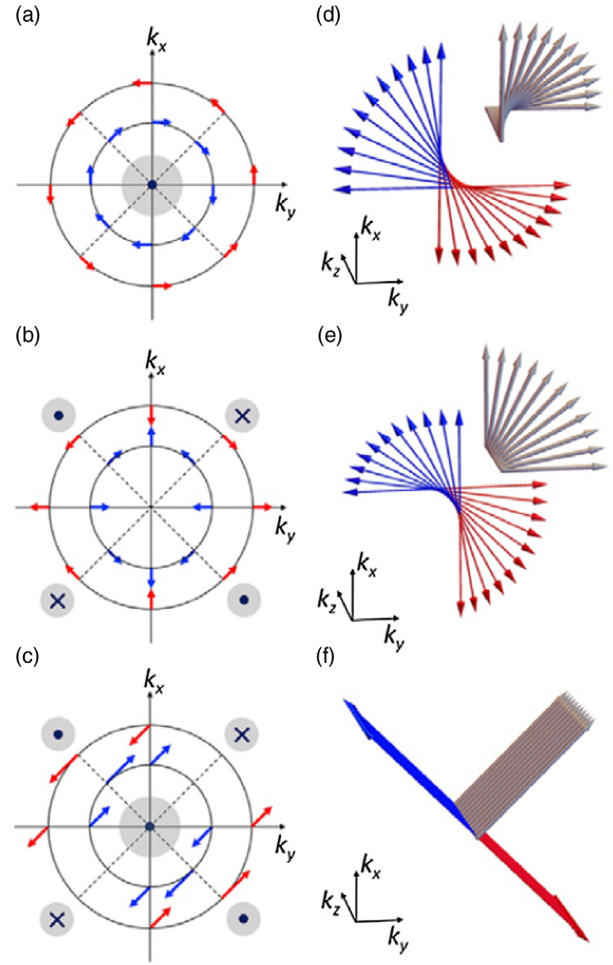


FIG. 1. (a) The orientations of the effective electrical field (light gray shaded circle) and spins (red and blue arrows) for the conventional Rashba SOC effect at surfaces or interfaces. (b) Same as (a) for the linear Dresselhaus effect in an asymmetry QW or a strained zinc-blende film. (c) Combined effect of (a) and (b). (d) The orientations of the effective electrical field (gray arrows) and spins (red and blue arrows) for the 1D SD-SOC effect as found in Ge. (e) Same as (d) as found in GaAs. (f) Combined effect of (d) and (e) as found in SiC.

where  $k_z$  is in units of  $\pi/c$ .  $\lambda_e$  ( $\lambda_c$ ) are the SOC strengths for the first (second) term. These two terms are found to correspond to the SD-SOC Hamiltonian in elemental and compound semiconductors with high ionicity, respectively, as shown later. A key difference between Eqs. (2) and (1) is a sinusoidal dependence of the effective field and hence spin texture on  $k_z$ , which results in a spin rotation in the  $(k_x, k_y)$  plane with a period of  $\pi$ . By imposing the  $C_2$  rotation plus translation symmetry, we solve Eq. (2) to obtain the spin texture of the 1D SD-SOC [29]. The first term gives rise to the following spin orientation as a function of  $k_z$ ,

$$\vec{s}_{1,2} = \mp \sin \frac{k_z}{2} \hat{k}_x \pm \cos \frac{k_z}{2} \hat{k}_y, \quad (3a)$$

$$\theta_1 = \frac{\pi}{2} + \frac{k_z}{2}, \quad \theta_2 = -\frac{\pi}{2} + \frac{k_z}{2}, \quad (3b)$$

where subscripts 1 and 2 represent spin-up and spin-down, respectively.  $\theta$  is the angle between the spin and the  $k_x$  axis. Similarly, from the second term in Eq. (2),

$$\vec{S}_{1,2} = \pm \cos \frac{k_z}{2} \hat{k}_x \mp \sin \frac{k_z}{2} \hat{k}_y, \quad (4a)$$

$$\theta_1 = \pi - \frac{k_z}{2}, \quad \theta_2 = -\frac{k_z}{2}. \quad (4b)$$

When both terms are present with equal strength, one has

$$\theta_1 = \frac{3\pi}{4}, \quad \theta_2 = -\frac{\pi}{4}. \quad (5)$$

These results lead to spin textures with spins rotating within one of the four quadrants, as shown in Figs. 1(d) and 1(e) for the first and second terms in Eq. (2), respectively. They differ by a phase of  $\pi/2$  [Fig. 1(d) vs Fig. 1(e)]. A very interesting case is when both terms are present with equal strength, then the effective field and hence the spin orientation becomes fixed along the diagonal direction of a quadrant independent of  $k_z$ , as shown in Fig. 1(f).

There are significant implications of different spin textures, as shown in Fig. 1. In a solid, due to the spin-momentum locking property, spin will rotate when electrons are scattered with a sudden change of momentum, leading to spin relaxation and a shortened spin coherence time. For the conventional 2D RD-SOC [Figs. 1(a) and 1(b)], spins can rotate in four quadrants in the  $(k_x, k_y)$  plane with an angle changing from 0 to  $2\pi$ . In contrast, for the newly discovered 1D SD-SOC [Figs. 1(d) and 1(f)], spins only rotate in one quadrant with an angle changing from 0 to  $\pi/2$ . Consequently, the 1D SD-SOC will exhibit a significant higher degree of spin coherency because the spins are constrained to vary within a much narrower range of angles. Furthermore, it is known that, for the 2D RD-SOC, an ideal spin texture [Fig. 1(c)] can be engineered by including both the first and second terms in Eq. (1) with equal strength, such as in a III-V heterostructure [37]. Similarly, an ideal spin texture can be achieved with the 1D SD-SOC [Fig. 1(e)], albeit be available intrinsically in a single material.

Next, to confirm the above theoretical analysis, we will characterize and quantify the 1D SD-SOC effects in several representative semiconductors with different ionicity, including Ge (Si), GaAs, and SiC, using first-principles density-functional theory and the tight-binding (TB) model Hamiltonian calculations [29]. Furthermore, to support our theoretical studies, we will demonstrate an experimental approach to show the feasibility of controlled formation of SDs in Si [29].

We first present the atomic and electronic structures of SDs in Ge, GaAs, and SiC for comparison, as shown in Fig. 2. Because of the larger SOC effect in Ge, we will show the results of Ge, while leaving the results of Si to be shown in Fig. S2 of the Supplemental Material [29]. The SDs are known to induce deep in-gap defect levels, as shown in Figs. 2(d)–2(f). Excluding SOC in the calculation, the two in-gap bands are spin degenerate, with charge distributions that are solely determined by the Ge, GaAs, or SiC atoms in the dislocation core [29]. Time reversal symmetry (TRS) ensures  $E_\sigma(k) = E_{\bar{\sigma}}(-k)$  for Kramers doublets with opposite momenta and orthogonal spins. Including SOC, the spin degeneracy of the two defect bands is lifted, as shown in Figs. 2(d)–2(f). Consistent with the SOC strength, the spin splitting is larger in GaAs than in Ge and SiC.

In Fig. 3(a), we show the spin texture  $\vec{p}(\vec{k})$  of the SOC-lifted states induced by the SD in Ge. At the same  $k$ , the directions of spins of lower and higher energy bands are opposite. Within the same band, the spin texture satisfies the condition,  $\vec{p}(\vec{k}) = -\vec{p}(-\vec{k})$ , ensured by the TRS. The  $z$  component of the spin polarization is negligible compared with the  $x$  and  $y$  components. Most interestingly, in Fig. 3(b) we plot the spin orientation  $\theta$ , the angle between the spin and the  $+k_x$  axis, as a function of  $k_z$ . It clearly

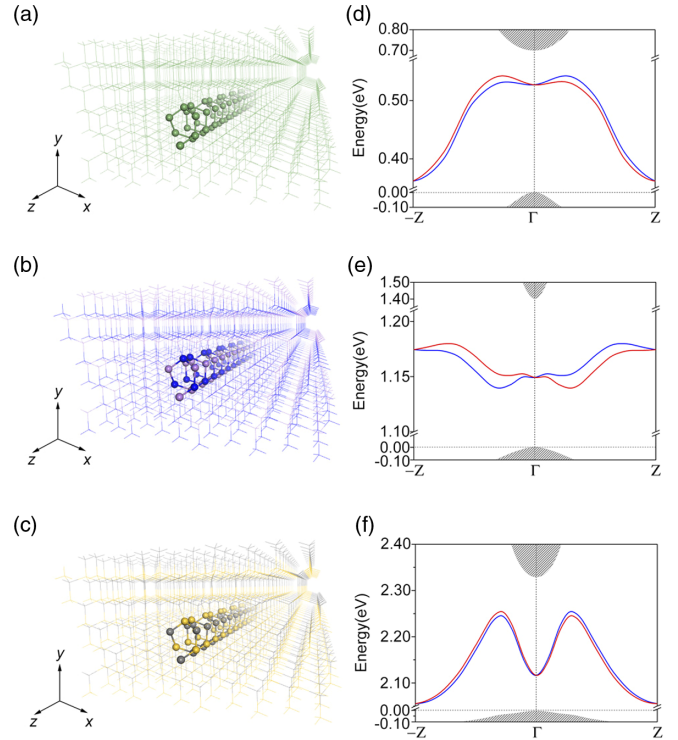


FIG. 2. (a)–(c) The atomic structures of a SD in bulk Ge, GaAs, and SiC, respectively. (d)–(f) Band structures of a SD in Ge, GaAs, and SiC with SOC effect, respectively. The Fermi level is set to zero. The red and blue lines represent SD-SOC bands with different spin projections.

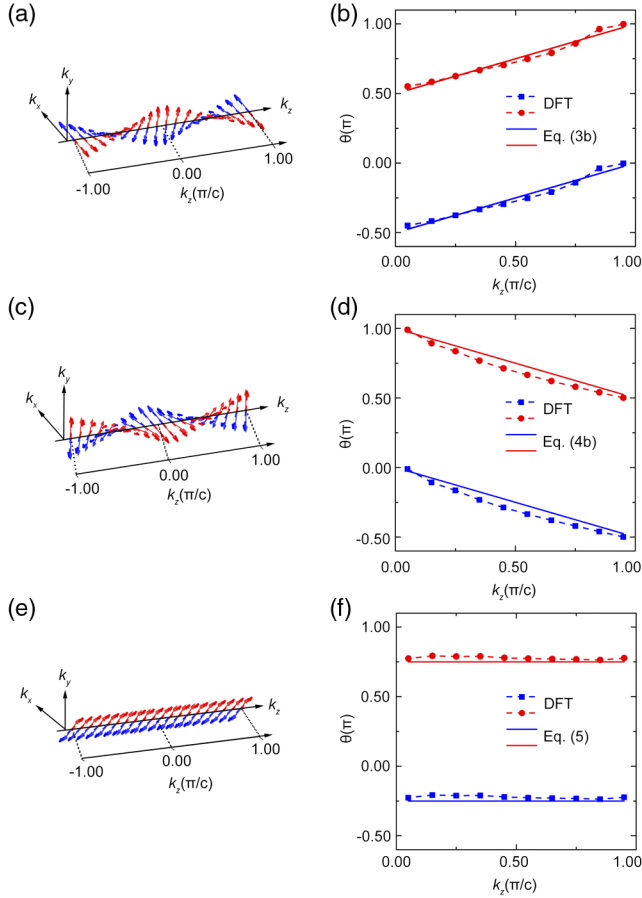


FIG. 3. (a),(c),(e) The spin textures of SD-SOC bands obtained from DFT calculations for Ge, GaAs, and SiC, respectively. The red and blue arrows show orientations of two spin projections. The dashed-line spin textures are obtained from TB results. (b), (d),(f) Data points (dots) show  $\theta$ , the angle between the spin and the  $+k_x$  axis, as a function of  $k_z$  obtained from DFT calculations for Ge, GaAs, and SiC, respectively. The lines are drawn according to Eqs. (3b), (4b), and (5), respectively.

shows a linear dependence following closely with Eq. (3b) as theoretically predicted from the first term of Eq. (2). This indicates that the SD in an elemental semiconductor generates a  $k_z$ -dependent local field pattern as depicted in Fig. 1(d). Therefore, generally, in a nonpolar elemental semiconductors with zero iconicity, the SOC arises from “structural” inversion symmetry breaking (in analogy to the Dresselhaus effect). It can be described by the first term in Eq. (2) and generates a spin texture following Eq. (3).

The calculated spin texture of SD in GaAs is shown in Fig. 3(c). Again the  $z$  component of the spin polarization is negligible. Interestingly, the spin texture is different from that of Ge, with the spin orientations phase shifted by  $\pi/2$ . As plotted in Fig. 3(d),  $\theta$  shows a linear dependence on  $k_z$ , closely following Eq. (4b), as theoretically predicted from the second term of Eq. (2). This indicates that the SD in a compound semiconductor with large ionicity generates a  $k_z$ -dependent local field pattern as depicted in Fig. 1(e).

Therefore, generally in compound semiconductors with large iconicity, the SOC arises from a local “electrical field” (in analogy to the Rashba effect). It can be described by the second term in Eq. (2) and generates a spin texture following Eq. (4).

The results for Ge and GaAs represent two extreme cases of an elemental semiconductor, with zero iconicity, and a compound semiconductor with large ionicity, respectively. Their spin textures correspond to the first and second term in Eq. (2), respectively, as shown above. We suppose that the SiC may be an intermediate case representing a system with medium iconicity. To test this hypothesis, we calculated the spin texture of SiC. Indeed the spin texture of SD in SiC, as shown in Figs. 3(e) and 3(f), is almost exactly the same as theoretically predicted in Eq. (5) and Fig. 1(f). The spin no longer rotates, but is fixed in the [110] direction. Therefore, generally, in compound semiconductors with medium ionicity, a SD generates a SOC effect as described by both the first and second terms in Eq. (2). It generates an ideal spin texture with spin conservation, which is predicted to be robust against all forms of spin-independent scattering [24,37,38]. Thus, the SD in those compound semiconductors with medium iconicity, like SiC, may be used effectively for suppressing spin relaxation in spintronics devices.

To support our theoretical studies, we will demonstrate an experimental approach to show the feasibility of controlled formation of SDs in Si (see Supplemental Material [29]). We have also calculated the stability of different SD structures and their corresponding SOC effects, which further confirmed the general applicability of our results and conclusions [29]. Because the unique spin texture of the 1D SD-SOC is induced by the intrinsic helical symmetry of the SD, all the properties we reveal here will be ubiquitous in semiconductors with SDs. To supplement our first-principles calculations, we have also constructed a general  $(2 \times 2)$  TB model Hamiltonian [see Eq. (S6) [29]] to extract the quantitative strength of SOC in different materials (Supplemental Material, Table S3) by fitting the TB bands to the first-principles bands [Figs. 3(a), 3(c), and 3(e) for spin texture and Fig. S4 for band structures, respectively]. For SiC, a semiconductor with middle iconicity ( $\lambda_c = \lambda_e$ ), it behaves as an intermediate (or average) effect of the first two. These results affirm again that the detailed spin texture can be tuned by the degree of iconicity with the same geometry of SDs or by different geometries of SDs. The latter deserves further investigation. Thus, effectively, a SD can act as a “SOC torque” to generate and conduct highly coherent spin currents, and SDs are therefore useful for spintronics device applications [24]. Especially, the SD in SiC is predicted to afford the most attractive test bed for future experiments, with an ideal form of SOC. The perspective of maximizing the strength of SOC in SDs [39] is also very appealing.

We thank S. B. Zhang, S.-H. Wei, and X. W. Zhang for helpful discussions. L.H. and B.H. acknowledge the

support from the Science Challenge Project (No. TZ2016003), China Postdoctoral Science Foundation (No. 2017M610754), NSFC (Grants No. 11574024 and No. 11704021), and NSAF (No. U1530401). H. H., W. J., X. N., Y. Z., and F. L. acknowledge the support from U.S. DOE (Award No. DE-FG02-04ER46148). The work of V. Z. and M. G. L. was supported in part by NSF (Grants No. DMR-9632527 and No. DMR-9304912), DOE (Award No. DE-FG02-00ER45816), and the Alexander von Humboldt Foundation. Computations were performed at Tianhe2-JK at CSRC.

L. H. and H. H. contributed equally to this work.

\*Corresponding author.

bing.huang@csrc.ac.cn

†Corresponding author.

fliu@eng.utah.edu

‡Present address: Institute of Applied and Physical Chemistry, University of Bremen, Bremen, D-28359, Germany.

- [1] J. P. Hirth and J. Lothe, *Theory of Dislocations* (Wiley, New York, 1982).
- [2] F. R. N. Nabarro, *Theory of Crystal Dislocations* (Oxford University Press, London, 1967).
- [3] H. M. Ng, D. Doppalapudi, and T. D. Moustakas, *Appl. Phys. Lett.* **73**, 821 (1998).
- [4] N. G. Weimann and L. F. Eastman, *J. Appl. Phys.* **83**, 3656 (1998).
- [5] D. C. Look and J. R. Sizelove, *Phys. Rev. Lett.* **82**, 1237 (1999).
- [6] M. Li, Z. Ding, Q. Meng, J. Zhou, Y. Zhu, H. Liu, M. S. Dresselhaus, and G. Chen, *Nano Lett.* **17**, 1587 (2017).
- [7] M. Li, Q. Song, T. Liu, L. Meroueh, G. D. Mahan, M. S. Dresselhaus, and G. Chen, *Nano Lett.* **17**, 4604 (2017).
- [8] Y. Ran, Y. Zhang, and A. Vishwanath, *Nat. Phys.* **5**, 298 (2009).
- [9] F. Liu, in *Handbook of Theoretical and Computational Nanotechnology*, edited by M. Rieth and W. Schommers (American Scientific Publishers, Stevenson Ranch, 2006), Chap. 10, p. 577.
- [10] F. M. Ross, R. Hull, D. Bahnck, J. C. Bean, L. J. Peticolas, and C. A. King, *Appl. Phys. Lett.* **62**, 1426 (1993).
- [11] L. M. Giovane, H.-C. Luan, A. M. Agarwal, and L. C. Kimerling, *Appl. Phys. Lett.* **78**, 541 (2001).
- [12] T. Kaplan, F. Liu, M. Mostoller, M. F. Chisholm, and V. Milman, *Phys. Rev. B* **61**, 1674 (2000).
- [13] E. Rashba, *Sov. Phys. Solid State* **2**, 1109 (1960).
- [14] G. Dresselhaus, *Phys. Rev.* **100**, 580 (1955).
- [15] K. Ishizaka *et al.*, *Nat. Mater.* **10**, 521 (2011).
- [16] D. Di Sante, P. Barone, R. Bertacco, and S. Picozzi, *Adv. Mater.* **25**, 509 (2013).
- [17] C. Rinaldi, S. Varotto, M. Asa, J. Sławińska, J. Fujii, G. Vinai, S. Cecchi, D. Di Sante, R. Calarco, I. Vobornik, G. Panaccione, S. Picozzi, and R. Bertacco, *Nano Lett.* **18**, 2751 (2018).
- [18] S. LaShell, B. A. McDougall, and E. Jensen, *Phys. Rev. Lett.* **77**, 3419 (1996).
- [19] D. Popovic, F. Reinert, S. Hufner, V. G. Grigoryan, M. Springborg, H. Cercellier, Y. Fagot-Revurat, B. Kierren, and D. Malterre, *Phys. Rev. B* **72**, 045419 (2005).
- [20] A. Varykhalov, D. Marchenko, M. R. Scholz, E. D. L. Rienks, T. K. Kim, G. Bihlmayer, J. Sánchez-Barriga, and O. Rader, *Phys. Rev. Lett.* **108**, 066804 (2012).
- [21] Y. M. Koroteev, G. Bihlmayer, J. E. Gayone, E. V. Chulkov, S. Blugel, P. M. Echenique, and P. Hofmann, *Phys. Rev. Lett.* **93**, 046403 (2004).
- [22] K. Sugawara, T. Sato, S. Souma, T. Takahashi, M. Arai, and T. Sasaki, *Phys. Rev. Lett.* **96**, 046411 (2006).
- [23] J. H. Dil, F. Meier, J. Lobo-Checa, L. Patthey, G. Bihlmayer, and J. Osterwalder, *Phys. Rev. Lett.* **101**, 266802 (2008).
- [24] A. Manchon, H. C. Koo, J. Nitta, S. M. Frolov, and R. A. Duine, *Nat. Mater.* **14**, 871 (2015).
- [25] R. Winkler, *Spin-Orbit Coupling Effects in Two-Dimensional Electron and Hole Systems* (Springer, New York, 2003).
- [26] J. Nitta, T. Akazaki, H. Takayanagi, and T. Enoki, *Phys. Rev. Lett.* **78**, 1335 (1997).
- [27] S. V. Ereameev, I. A. Nechaev, Y. M. Koroteev, P. M. Echenique, and E. V. Chulkov, *Phys. Rev. Lett.* **108**, 246802 (2012).
- [28] M. I. Dyakonov and V. Yu. Kachorovskii, *Sov. Phys. Semicond.* **20**, 110 (1986).
- [29] See Supplemental Materials at <http://link.aps.org/supplemental/10.1103/PhysRevLett.121.066401> for more details about computational methods, derivation of the 1D SOC Hamiltonian, some other electronic properties of different SDs, TB model calculation, and experimental feasibility, which includes Refs. [30–36].
- [30] G. Kresse and J. Furthmüller, *Comput. Mater. Sci.* **6**, 15 (1996).
- [31] J. P. Perdew, K. Burke, and M. Ernzerhof, *Phys. Rev. Lett.* **77**, 3865 (1996).
- [32] J. Heyd, G. E. Scuseria, and M. Ernzerhof, *J. Chem. Phys.* **118**, 8207 (2003).
- [33] A. T. Blumenau, R. Jones, and T. Frauenheim, *J. Phys. Condens. Matter* **15**, S2951 (2003).
- [34] V. Zielasek, F. Liu, Y. Zhao, J. B. Maxson, and M. G. Lagally, *Phys. Rev. B* **64**, R201320 (2001).
- [35] O. L. Alerhand, D. Vanderbilt, R. D. Meade, and J. D. Joannopoulos, *Phys. Rev. Lett.* **61**, 1973 (1988).
- [36] H. C. Koo, J. H. Kwon, J. Eom, J. Chang, S. H. Han, and M. Johnson, *Science* **325**, 1515 (2009).
- [37] N. S. Averkiev and L. E. Golub, *Phys. Rev. B* **60**, 15582 (1999).
- [38] J. Schliemann, J. C. Egues, and D. Loss, *Phys. Rev. Lett.* **90**, 146801 (2003).
- [39] V. Sunko, H. Rosner, P. Kushwaha, S. Khim, F. Mazzola, L. Bawden, O. J. Clark, J. M. Riley, D. Kasinathan, M. W. Haverkort, T. K. Kim, M. Hoesch, J. Fujii, I. Vobornik, A. P. Mackenzie, and P. D. C. King, *Nature (London)* **549**, 492 (2017).